Stochastic model for a vortex depinning in random media

Byungnam Kahng, Kwangho Park, and Jinhee Park
Department of Physics and Center for Advanced Materials and Devices, Kon-Kuk University, Seoul 143-701, Korea
(Received 8 July 1997; revised manuscript received 2 December 1997)

We present a self-organized stochastic model for the dynamics of a single flux line in random media. The dynamics of the flux line in the longitudinal and the transverse direction to average velocity direction are coupled to each other. The roughness exponents of the flux line are measured for each direction, which are $\alpha_{\parallel} \approx 0.63$ for the longitudinal and $\alpha_{\perp} \approx 0.5$ for the transverse direction, respectively. The dynamic exponents are obtained as $z \approx 1$ for both directions. We also examine the avalanche size distribution, which exhibits a power-law behavior with the exponent consistent with the one for the Sneppen model in 1+1 dimensions. [S1063-651X(98)11703-8]

PACS number(s): 05.40.+j, 68.35.Fx, 64.60.Ht

In the past few years, there has been an explosion of studies in the field of dynamics of fluctuating interfaces due to theoretical interests in the classification of universality for stochastic models and also due to applications to various physical phenomena such as crystal growth, vapor deposition, electroplating, biological growth, etc. A number of discrete models and continuum equations for interface dynamics have been introduced and studied [1–3]. An interesting feature of nonequilibrium interface dynamics is the nontrivial dynamic scaling behavior [4] of the interface fluctuation width, i.e.,

$$W(L,t) = \left\langle \frac{1}{L^{d'}} \sum_{x} [h(x,t) - \overline{h}(t)]^2 \right\rangle^{1/2} \sim L^{\alpha} f(t/L^{z}), \quad (1)$$

where $h(x,t)$ is the height of site x on the substrate at time t. $\overline{h}$, L, and d' denote the mean height, system size, and substrate dimension, respectively. The angular brackets stand for statistical average. The scaling function behaves as $f(x) \to \text{const}$ for $x \gg 1$, and $f(x) \sim x^{\beta}$ for $x \ll 1$ with $z = \alpha/\beta$. The exponents α, β, and z are called the roughness, the growth, and the dynamic exponents, respectively.

Recently the problem of the pinning-depinning (PD) transition of interfaces in random media has also attracted interest in association with the dynamics of fluctuating interfaces in random media. Examples include the dynamics of domain boundaries of random Ising spin systems after being quenched below the critical temperature [5], wetting immiscible displacement of one fluid by another in a porous medium [6,7], pinning flux lines in type-II superconductors [8,9], fluid imbibition in paper [10], etc. In the problem of the PD transition, the interface is pinned when external driving force F is weaker than pinning strength induced by random media, while it moves with a certain velocity v when the force F is greater than the pinning strength. Thus there exists a threshold of external applied force F_c across which the PD transition occurs. The role of the order parameter is played by the mean velocity, $v = \langle \Sigma_x \partial h(x,t)/\partial t \rangle / L^{d'}$. Accordingly, the velocity is zero for $F < F_c$, and increases for $F > F_c$ as $v \sim (F - F_c)^{\theta}$, where the exponent θ is called the velocity exponent.

The continuum equation for the dynamics of interfaces in random media may be written simply as [7]

$$\frac{\partial h(x,t)}{\partial t} = \nu \nabla^2 h + F + \eta(x,h), \quad (2)$$

where $h(x,t)$ is the height of the interface at position x at time t. The first term on the right-hand side is from the smoothening effect of surface tension, the second term the uniform driving force, and the third a random force with short range correlations, satisfying $\langle \eta(x,h) \rangle = 0$ and $\langle \eta(x,h)\, \eta(x',h') \rangle = 2D\, \delta(x-x')\, \delta(h-h')$ with noise strength D. The above equation, called the quenched Edwards-Wilkinson (QEW) equation, would be relevant to the dynamics of the domain wall in random magnetic systems. More generally, recently a new continuum equation was introduced [11], which includes a nonlinear term $(\lambda/2)(\nabla h)^2$ induced from the anisotropic property of the pinning strength. Thus the equation is replaced by

$$\frac{\partial h(x,t)}{\partial t} = \nu \nabla^2 h + \frac{\lambda}{2} (\nabla h)^2 + F + \eta(x,h), \quad (3)$$

which is called the quenched Kardar-Parisi-Zhang (QKPZ) equation. The QKPZ equation leads to a different universality class from the QEW equation. Recently several stochastic models in the QKPZ universality class have been introduced [10,12]. From the models, it has been naturally concluded that the surface at the threshold of the PD transition F_c can be described by the directed percolation (DP) cluster spanned perpendicularly to the surface growth direction in 1+1 dimensions. The roughness exponent α of the interface is given as the ratio of the correlation length exponents $\nu_{\perp}$ and $\nu_{\parallel}$ of the DP cluster in the transverse and the longitudinal direction that is $\alpha = \nu_{\perp}/\nu_{\parallel} \approx 0.63$.

The dynamics of a single flux line in a type-II superconductor with random impurities can also be understood in a similar manner used in the dynamics of surface growth. The main difference between them lies in that the flux line is a one-dimensional chain embedded in three dimensions rather than in two dimensions. Thus the roughness of the flux line is quantified in two different directions, the longitudinal and the transverse to average velocity direction. Recently the

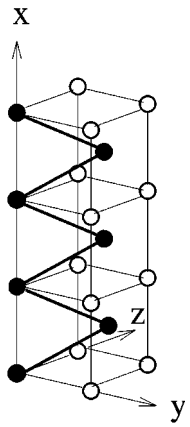

FIG. 1. The initial flat configuration of the discrete version of elastic string. Each bead has two-component noises representing random pinning forces in the y and z directions.

continuum equations for the flux line dynamics in each directions were derived by Ertas and Kardar [8,9], which are coupled to each other and look very complicated in general. They obtained the roughness and the dynamic exponents for various cases of the coupled equations; however, there still remain several cases where the roughness and dynamic exponents are not determined yet. In this paper, we will introduce a simple self-organized stochastic model, which might be relevant to the dynamics of the flux line. The numerical results we obtain from the stochastic model might make up for the list of the roughness and the dynamic exponents in Ref. [9].

The stochastic model we introduce in this paper is defined as follows. First, we consider a body centered cubic (bcc) lattice, in which an elastic string runs along the x direction as shown in Fig. 1. The discrete version of the elastic string is composed of L-massless beads (black dots), which locate at nearest neighboring sites of one another and are connected through strings. The zigzag-type configuration as shown in Fig. 1 is regarded as an initial flat configuration. The total length of the string is equal to $\sqrt{3}aL/2$, where a is the unit lattice constant of the bcc lattice and L is the total number of beads in the system. The elastic string does not run backward to the x direction, so that (y,z) positions of the bead for each x are specified by single values. Each bead is allowed to update only in either the positive y or positive z direction according to the following rule. First, two random numbers are assigned on each bead, one of which is for the positive y direction and the other is for the positive z direction. The random numbers for the y direction are uniformly distributed between $[0,p]$ where $p \leqslant 1$ and the ones for the z direction are in $[0,1]$. Next, a minimum random number is selected among the $2L$ random numbers of the entire system, through which we determine the position and the direction of bead to move. Then the bead having the minimum random number is updated by shifting its position by the lattice constant a along the direction chosen. Next, the avalanche process of updating may occur on neighboring beads when the separation between the nearest neighboring beads along the string becomes larger than $\sqrt{3}a/2$. In that case, the nearest neighboring bead is also shifted by a lattice constant along the direction already selected. The avalanche rule is then applied successively to next neighboring beads to conserve the separation between nearest neighboring beads. Finally, the random numbers at the newly updated sites are replaced by new ones in both y and z directions. Thus it is possible that a random number at a certain site in one direction can be replaced without changing its position when the position in the other direction is updated. The dynamic rule we used is similar to the Sneppen dynamic rule [13] but the updating occurs in two different directions. Accordingly, we call our model the vector Sneppen model hereafter.

It would be interesting to derive the continuum equation for the vector Sneppen model. The derivation of the continuum equation is based on the coarse-grained description rather than through the stochastic approach using the master equation. In fact, our derivation follows that used by Ertas and Kardar in Ref. [9] but the external driving force is not given via external current. The equation of motion is obtained by balancing the conservative and dynamical forces affected on the flux line. The conservative force consists of the elastic force, driving force, and random force due to impurities. The dynamical force is proportional to the local velocity of the flux line in the normal direction. Let the position of flux line at substrate position x and time t in three-dimensional space be denoted by $\vec{R}(x,t)$. In order to specify the normal velocity for the flux line, one first defines local tangent vector,

$$\hat{t} = \frac{1}{\sqrt{g}} \partial_x \vec{R}, \tag{4}$$

where g is the metric. Then one defines a projection operator,

$$\mathcal{P}_{ij} \equiv \delta_{ij} - \hat{t}_i \hat{t}_j . \tag{5}$$

Using the above two quantities, one can write the velocity in the normal direction as

$$\vec{v}_n = \mathcal{P} \cdot \partial_t \vec{R} = \partial_t \vec{R} - (\partial_t \vec{R} \cdot \hat{t}) \hat{t}, \tag{6}$$

where $\mathcal{P} = \{\mathcal{P}_{ij}\}$ is the projector operator. The conservative force acting in the normal direction is given as

$$\vec{\mathcal{F}}_n = \mathcal{P} \cdot \{\partial_x{}^2 \vec{R} + \vec{F} + \vec{f}\}, \tag{7}$$

where the first term on the right-hand side is from the elastic force of the flux line, the second term is the uniform driving force, and the third is a random force with short range correlation. Then the equation of motion can be obtained by balancing Eq. (6) and Eq. (7) as

$$\eta \mathcal{P} \cdot \partial_t \vec{R} = \vec{\mathcal{F}}_n , \tag{8}$$

where η is viscosity. Next, $\{\hat{x}, \hat{e}_\parallel, \hat{e}_\perp\}$ is taken as the basis vector of the coordinate system, where $\hat{e}_\parallel$ is selected as the direction of average velocity that is parallel to applying force. Then the flux line is represented as $\vec{R}(x,t) = x\hat{x} + r_\parallel(x,t)\hat{e}_\parallel + r_\perp(x,t)\hat{e}_\perp$, and the metric is given as $g = 1 + (\partial_x r_\parallel)^2 + (\partial_x r_\perp)^2$. Obviously $\vec{F} = F\hat{e}_\parallel$, and the random

eforce is represented as $\vec{f}=f_x\hat{x}+f_\parallel\hat{e}_\parallel+f_\perp\hat{e}_\perp$. Then the equations of motion for the flux line in $r_\parallel$ and $r_\perp$ directions become

$$\frac{\eta\partial_t r_\parallel}{\sqrt{1+s_\parallel{}^2}}=\partial_x{}^2 r_\parallel+\frac{\lambda_{1\parallel}}{2}s_\parallel{}^2+\frac{\lambda_{1\perp}}{2}s_\perp{}^2+F+\tilde{f}_\parallel, \tag{9}$$

$$\frac{\eta\partial_t r_\perp}{\sqrt{1+s_\perp{}^2}}=\partial_x{}^2 r_\perp+\tilde{f}_\perp, \tag{10}$$

where $s_\parallel\equiv\partial_x r_\parallel$, $s_\perp\equiv\partial_x r_\perp$, and the random forces are

$$\tilde{f}_\parallel=\frac{(f_\parallel-s_\parallel f_x)}{\sqrt{1+s_\parallel{}^2}}, \tag{11}$$

$$\tilde{f}_\perp=\frac{(f_\perp-s_\perp f_x)}{\sqrt{1+s_\perp{}^2}}. \tag{12}$$

The remaining parameters are given by $\lambda_{1\parallel}=-F$ and $\lambda_{1\perp}=2F$, which are nonzero for $F\neq 0$. Note that Eq. (10) is invariant under $r_\perp\to -r_\perp$. According to the presence of the nonlinear term, $(\lambda_{1\parallel}/2)s_\parallel^2$ in Eq. (9), the dynamics of the longitudinal direction is expected to belong to the quenched KPZ universality class, while for the transverse direction, the dynamics would be in a new universality class. This is because Eq. (10) does not include external force, but is affected by the longitudinal dynamics through the random noise, so that the quenched Edwards-Wilkinson universality is excluded. Equations (9) and (10) would be a special case of the equations presented by Ertas and Kardar in Ref. [9],

$$\partial_t r_\alpha=\mu_{\alpha\beta}F_\beta+\kappa_{\alpha\beta}\partial_x r_\beta+K_{\alpha\beta}\partial_x{}^2 r_\beta \times\tfrac{1}{2}\lambda_{\alpha,\beta\gamma}\partial_x r_\beta\partial_x r_\gamma+f_\alpha, \tag{13}$$

where α and β denote either $\parallel$ or $\perp$.

In order to obtain the roughness exponents for each direction, we consider the spatial correlation functions $C_\parallel$ and $C_\perp$ after saturation,

$$C_\parallel(x,t)=\left\langle\frac{1}{L}\sum_{x_1}[r_\parallel(x+x_1,t)-r_\parallel(x_1,t)]^2\right\rangle^{1/2},$$

$$C_\perp(x,t)=\left\langle\frac{1}{L}\sum_{x_1}[r_\perp(x+x_1,t)-r_\perp(x_1,t)]^2\right\rangle^{1/2}, \tag{14}$$

which behave as $C_\parallel(x)\sim x^{\alpha_\parallel}$ and $C_\perp(x)\sim x^{\alpha_\perp}$. Next, in order to obtain the growth exponents, we consider the temporal correlation functions $\tilde{C}_\parallel$ and $\tilde{C}_\perp$,

$$\tilde{C}_\parallel(t_2-t_1)=\left\langle\frac{1}{L}\sum_{x}[r_\parallel(x,t_2)-\overline{r_\parallel}(t_2)-r_\parallel(x,t_1)+\overline{r_\parallel}(t_1)]^2\right\rangle^{1/2},$$

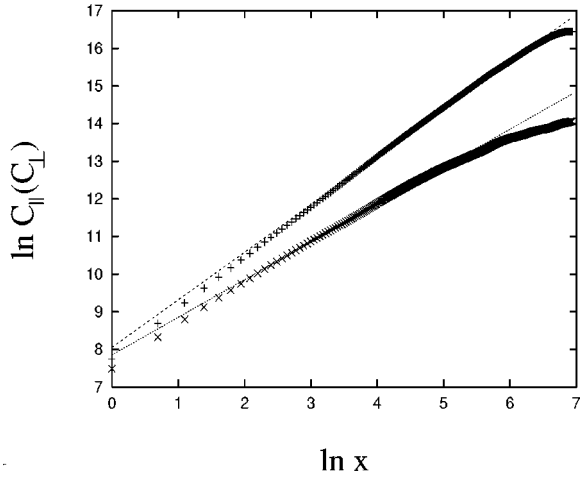

FIG. 2. Plot of $C_\parallel$ ($C_\perp$) vs x for $p=1$ in double logarithmic scales. The simulations were performed for system size $L=2048$. The lines obtained from the least square fits have the slopes 1.26 (top) and 1.00.

$$\tilde{C}_\perp(t_2-t_1)=\left\langle\frac{1}{L}\sum_{x}(r_\perp(x,t_2)-\overline{r_\perp}(t_2)-r_\perp(x,t_1)+\overline{r_\perp}(t_1))^2\right\rangle^{1/2}, \tag{15}$$

where t_1 is taken as a time in steady state. The correlation functions behave as $\tilde{C}_\parallel\sim(t_2-t_1)^{\beta_\parallel}$ and $\tilde{C}_\perp\sim(t_2-t_1)^{\beta_\perp}$. Numerical simulations were performed for the cases of $p=1$ and $p=1/2$.

For $p=1$, the roughness exponents are measured as $\alpha_\parallel\approx 0.63$ and $\alpha_\perp\approx 0.50$ as shown in Fig. 2. The growth exponents are measured as $\beta_\parallel\approx 0.64$ and $\beta_\perp\approx 0.53$ as shown in Fig. 3. From the numerical results, the dynamic exponents are obtained as $z_\parallel\approx 0.99$ and $z_\perp\approx 0.95$, which suggest that the true dynamic exponents are $z_\parallel=z_\perp=1$. This result may be attributed to the fact that the coherent effect propagates along the string and the chemical distance between any two

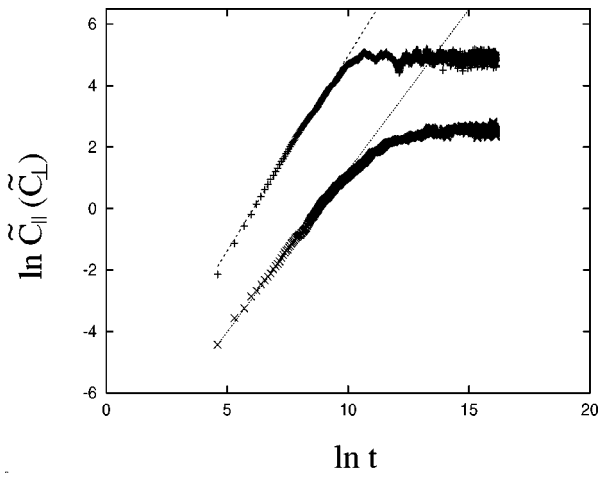

FIG. 3. Plot of $\tilde{C}_\parallel$ ($\tilde{C}_\perp$) vs time for $p=1$ in double logarithmic scales. The simulations were performed for system size $L=2048$. The lines obtained from the least square fits have the slopes 1.27 (top) and 1.05.

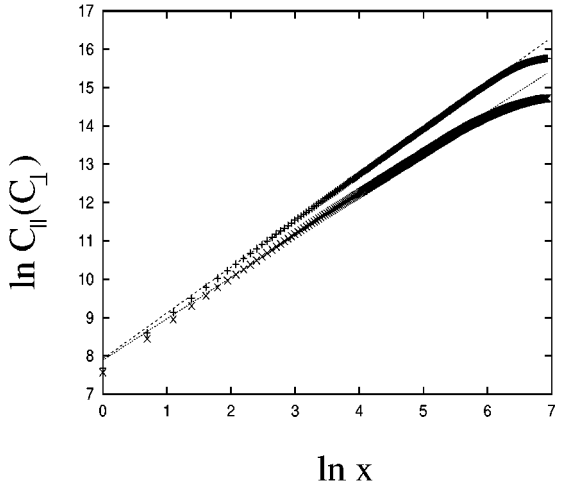

FIG. 4. Plot of $C_{\parallel}$ ($C_{\perp}$) vs x for $p=1/2$ in double logarithmic scales. The simulations were performed for system size $L=2048$. The lines obtained from the least square fits have the slopes 1.20 (top) and 1.08.

points on the string remains invariant under the restricted solid-on-solid condition [14]. Next, for $p=1/2$, the spatial correlation functions for each direction are less distinctive than the case of $p=1$ as shown in Fig. 4. The roughness exponents were obtained as $\alpha_{\parallel}\approx 0.60$ and $\alpha_{\perp}\approx 0.54$. For the growth exponents, it is likely that the time correlation function $\tilde{C}_{\parallel}$ in the longitudinal direction exhibits a power-law behavior against time with $\beta_{\parallel}\approx 0.64$. However, for the transverse direction, the data do not exhibit a simple power-law type behavior, rather they show a crossover behavior from $\beta_{\perp}\approx 0.50$ to $\beta_{\perp}<0.50$ in Fig. 5. One may see the crossover as a long transient behavior. From the numerical results, it is suggested that the roughness exponents are $\alpha_{\parallel}=0.63$ and $\alpha_{\perp}=0.5$, and the dynamic exponents are $z_{\parallel}=z_{\perp}=1$ for the values of $0<p\leqslant 1$. Note that when $p=0$, the dynamics in the transverse direction does not occur, and the model reduces to the ordinary Sneppen model. Accordingly, the numerical results indicate that the roughness and dynamic exponents are independent of p. This point can also be

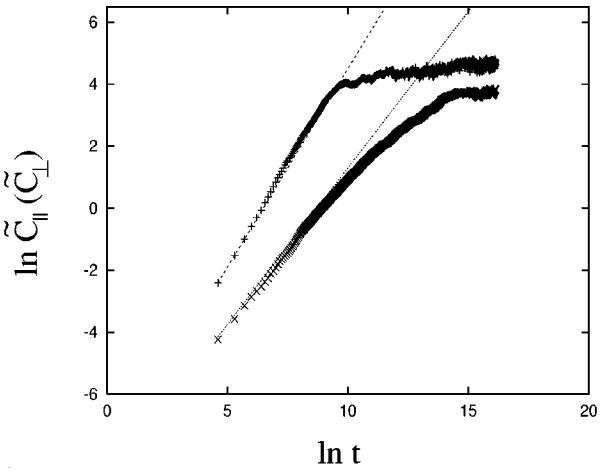

FIG. 5. Plot of $\tilde{C}_{\parallel}$ ($\tilde{C}_{\perp}$) vs time for $p=1/2$ in double logarithmic scales. The simulations were performed for system size $L=2048$. The lines have the slopes 1.28 (top) and 1.00.

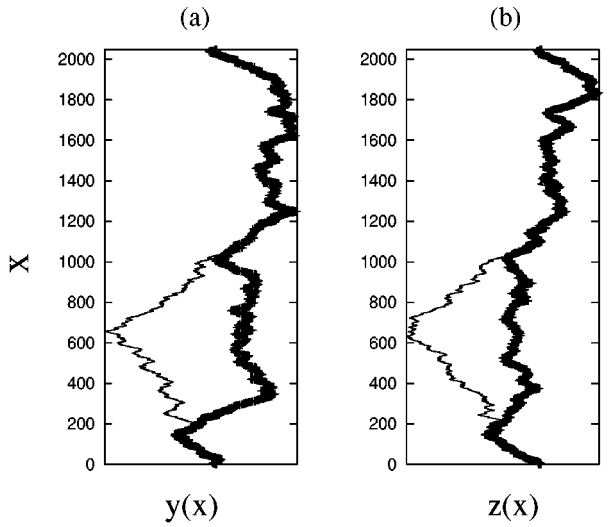

FIG. 6. Snapshots of a flux line for different times (a) in the y direction and (b) in the z direction for $p=1.0$. The thicker curves are for 5 Monte Carlo steps later.

confirmed by the fact that Eqs. (9) and (10) do not include any factor depending on the angle between average velocity direction and the y direction. The numerical values of the roughness and dynamic exponents for the longitudinal direction $\alpha_{\parallel}\approx 0.63$ and $z_{\parallel}\approx 1$ suggest that the dynamics belongs to the directed percolation depinning universality class (the QKPZ universality class) in $1+1$ directions. On the other hand, for the transverse direction, the numerical values $\alpha_{\perp}\approx 0.5$ and $z_{\perp}\approx 1$ leads to a new universality.

Next, let us consider the properties of self-organized criticality [16] for the vector Sneppen model. As the case of the original Sneppen model, the dynamics of the vector Sneppen model evolves through the process of the coherent activity after a transient period. The coherent activity means newly updatings are much more likely to occur among the sites updated their random numbers. Through the avalanche pro-

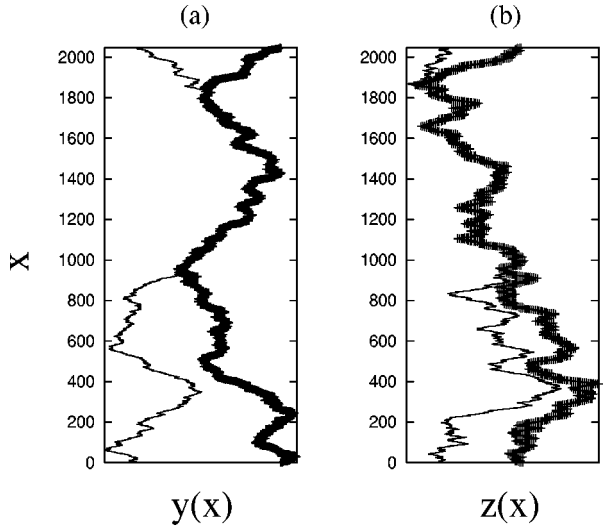

FIG. 7. Snapshots of a flux line for different times (a) in the y direction and (b) in the z direction for $p=0.5$. The thicker data are for 5 Monte Carlo steps later.

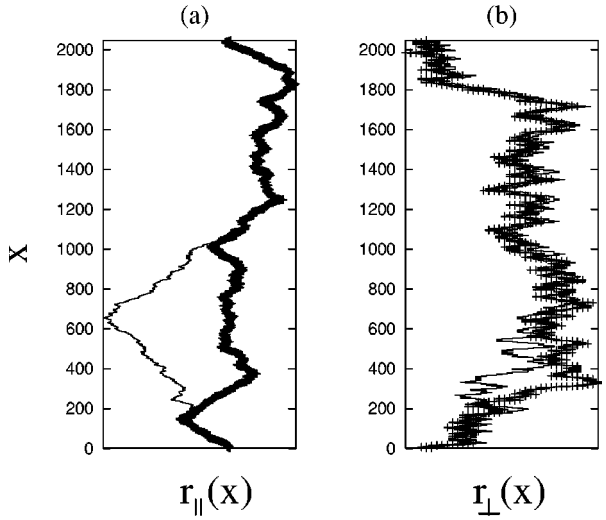

FIG. 8. Snapshots of a flux line for different times (a) in the longitudinal direction and (b) in the transverse direction for $p = 1.0$. The thicker data are for 5 Monte Carlo steps later.

cess, the active zones extend the boundary with increasing time. Figures 6 and 7, the snapshots of the flux lines, illustrate this feature. The areas of the active zones in the y and z directions are almost the same for $p = 1$, while the area in the y direction is much larger than the one of the z direction for $p = 0.5$. That is because minimum random numbers are more likely to be selected in the y direction, and updating occurs much more frequently in the y direction. However, the linear sizes of the active zones in the y and z directions are almost same, which implies that the self-organized critical phenomenon occurs coherently in both directions. Note that the random number at a certain site in one direction can change without its position when the position in the other direction is updated. In other words, the activity of updating or avalanches in one direction affects the activity in the other direction, which is the characteristics of the vector Sneppen model. Therefore the linear sizes of the active zone in each

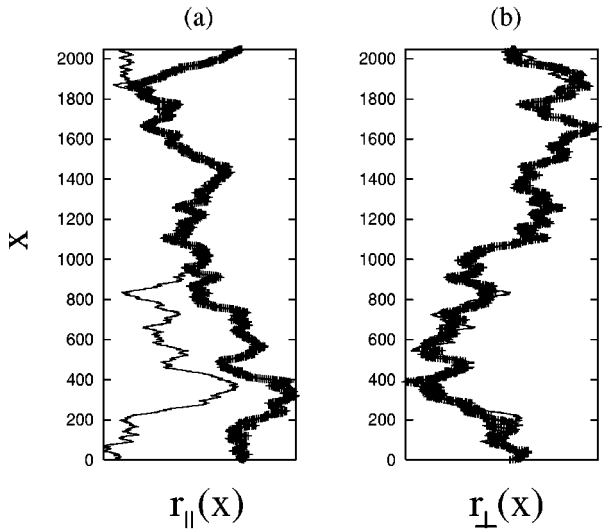

FIG. 9. Snapshots of a flux line for different times (a) in the longitudinal direction and (b) in the transverse direction for $p = 0.5$. The thicker data are for 5 Monte Carlo steps later.

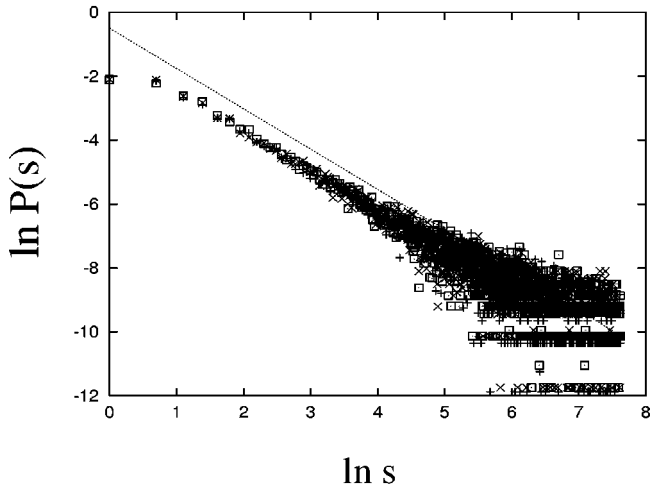

FIG. 10. Plot of the avalanche size distribution for $p = 1.0$. The symbol □ means the data of the y direction, x of the z direction, and + of the total. The data are accumulated over 150 configurations. The dotted line with the slope 1.26 was drawn to guide the eyes.

direction are almost the same. We plot the snapshots in the longitudinal and transverse directions in Figs. 8 and 9. In the longitudinal direction, the active zone is localized, and the dynamics through the associated process [17,18] can be obviously seen, while for the transverse direction, it is not obvious that the dynamics evolves through the associated process, and the active zone is not localized. From this sense, the dynamics of the vector Sneppen model in the transverse direction is different from the one for the anisotropic model proposed by Maslov and Zhang [15] where the active zone is localized and propagates anisotropically, but the values of the roughness and dynamic exponents are the same by accident for the two cases, the vector Sneppen model and the anisotropic KPZ model.

We examine the avalanche size distribution for the vector Sneppen model. The avalanche size is defined as the number

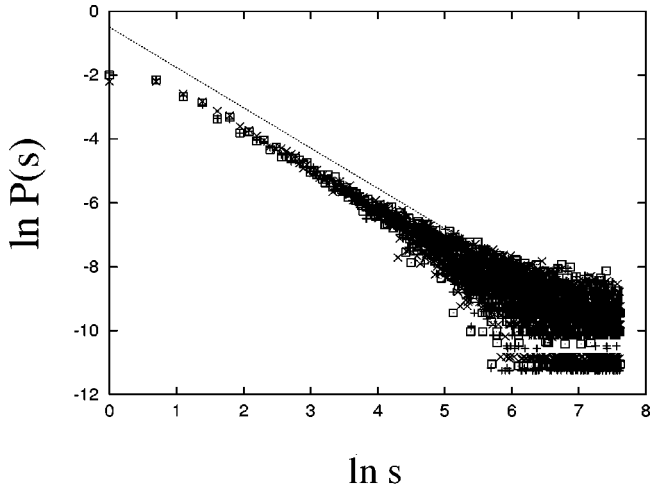

FIG. 11. Plot of the avalanche size distribution for $p = 0.5$. The symbol □ means the data of the y direction, x of the z direction, and + of the total. The data are accumulated over 200 configurations. The dotted line with the slope 1.26 was drawn to guide the eyes.

of sites that update their positions through the so-called associated process [16–18]. Since updatings occur in y and z directions, the associated process is counted in three different ways, the processes in each directions separately and the one in both the directions together. Minimum random numbers are also traced in three different ways. Accordingly, the avalanche size, which is the number of sites that update their positions during the interval of two successive increasing minimum random numbers, is also counted in three different ways. All the avalanche size distributions exhibit power-law behavior $P(s) \sim s^{-\tau}$ with the three exponents $\tau = \tau_y$, $\tau = \tau_z$, and $\tau = \tau_{\rm tot}$, in the y direction, the z direction, and in both directions, respectively. The power-law behavior appears much more clearly for the region of small avalanche sizes in Figs. 10 and 11. For large size region, the data are scattered, which reflects that large sized avalanches occur frequently. The occurrence of large sized avalanches implies the dynamic exponent $z = 1$. We measured the numerical values for the three exponents τ_x, τ_y, and $\tau_{\rm tot}$ for the cases of $p = 0.5$ and $p = 1$. All values of the exponents for each case are close to 1.26, which is the value of the exponent τ for the avalanche size distribution for the ordinary Sneppen model in $1+1$ dimensions.

In summary, we have introduced the vector Sneppen model associated with the dynamics of the flux line in quenched media at the depinning threshold. The roughness and dynamic exponents are obtained in the longitudinal and transverse directions, which are $\alpha_\parallel \approx 0.63$ $\alpha_\perp \approx 0.5$, and $z_\parallel = z_\perp \approx 1$. We have also investigated the avalanche size distributions where the avalanche sizes are counted in three different ways such that the y and z directions update separately and together. It was obtained that the exponents τ for the avalanche size distribution for the three cases are consistent with the one for the $(1+1)$-dimensional Sneppen model.

This work was supported in part by the Non-Directional Research Fund, Korea Research Foundation, in part by the KOSEF through the SRC program of SNU-CTP, and in part by the Ministry of Education (Grant No. BSRI 97-2409), Korea.

[1] For a recent review, see, for examples, F. Family and T. Vicsek, *Dynamics of Fractal Surfaces* (World Scientific, Singapore, 1991).
[2] A.-L. Barabási and H. E. Stanely, *Fractal Concepts in Surface Growth* (Cambridge University Press, Cambridge, England, 1995).
[3] D. Kim, H. Park, and B. Kahng, *Dynamics of Fluctuating Interfaces and Related Phenomena* (World Scientific, Singapore, 1997).
[4] F. Family, J. Phys. A **19**, L441 (1986).
[5] R. Bruinsma and G. Aeppli, Phys. Rev. Lett. **52**, 1547 (1984).
[6] M. A. Rubio, C. A. Edwards, A. Dougherty, and J. P. Gollub, Phys. Rev. Lett. **63**, 1685 (1989).
[7] D. Kessler, H. Levine, and Y. Tu, Phys. Rev. A **43**, 4551 (1991).
[8] D. Ertas and M. Kardar, Phys. Rev. Lett. **73**, 1703 (1994).
[9] D. Ertas and M. Kardar, Phys. Rev. B **53**, 3520 (1996).
[10] S. V. Buldyrev, A.-L. Barabási, F. Caserta, S. Havlin, H. E. Stanley, and T. Viscek, Phys. Rev. A **45**, R8313 (1992).
[11] L.-H. Tang, M. Kardar, and D. Dhar, Phys. Rev. Lett. **74**, 920 (1995).
[12] L.-H. Tang and H. Leschhorn, Phys. Rev. A **45**, R8309 (1992).
[13] K. Sneppen, Phys. Rev. Lett. **69**, 3539 (1992).
[14] S. Havlin, L. A. N. Amaral, S. V. Buldyrev, S. T. Harrington, and H. E. Stanley, Phys. Rev. Lett. **74**, 4205 (1995).
[15] S. Maslov and Y.-C. Zhang, Phys. Rev. Lett. **75**, 1550 (1995).
[16] M. Paczuski, S. Maslov, and P. Bak, Phys. Rev. E **53**, 414 (1996).
[17] Z. Olami, I. Procaccia, and R. Zeitak, Phys. Rev. E **49**, 1232 (1994); **52**, 3402 (1995).
[18] H. Leschhorn and L.-H. Tang, Phys. Rev. E **49**, 1238 (1994).